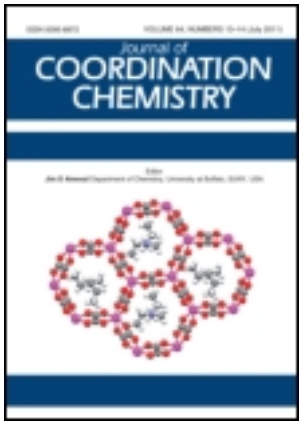

Journal of Coordination Chemistry
Publication details, including instructions for authors and subscription information:
http://www.tandfonline.com/loi/gcoo20

Triphenyltin chloride complexes containing bidentate organodiimines as effective antitumor agents

Ahmed S. Badr El-Din [a], Safaa El-Din H. Etaiw [a] & Mohamed E. El-Zaria [a]

[a] Chemistry Department, Faculty of Science, University of Tanta, Tanta, Egypt

Accepted author version posted online: 03 Sep 2012.Published online: 17 Sep 2012.

To cite this article: Ahmed S. Badr El-Din, Safaa El-Din H. Etaiw & Mohamed E. El-Zaria (2012) Triphenyltin chloride complexes containing bidentate organodiimines as effective antitumor agents, Journal of Coordination Chemistry, 65:21, 3776-3791, DOI: 10.1080/00958972.2012.725846

To link to this article: http://dx.doi.org/10.1080/00958972.2012.725846

Journal of Coordination Chemistry
Vol. 65, No. 21, 10 November 2012, 3776–3791

Triphenyltin chloride complexes containing bidentate organodiimines as effective antitumor agents

AHMED S. BADR EL-DIN, SAFAA EL-DIN H. ETAIW*
and MOHAMED E. EL-ZARIA

Chemistry Department, Faculty of Science, University of Tanta, Tanta, Egypt

(*Received 26 May 2012; in final form 10 August 2012*)

Three triphenyltin chloride complexes, $[(Ph_3SnCl)_2 \cdot (bpy)_{1.5}]$ (**1**), $[(Ph_3SnCl)_2.tbpe]$ (**2**), and $[(Ph_3SnCl)_2 \cdot bpe]$ (**3**), were synthesized by reaction of triphenyltin chloride with 4,4′-bipyridine (bpy), *trans*-1,2-bis(4-pyridyl)ethylene (tbpe), and 1,2-bis(4-pyridyl)ethane (bpe) in water/acetonitrile. Both **2** and **3** are binuclear; each consists of two Ph_3SnCl molecules bridged by the bidentate ligand. Complex **1** consists of two crystallographically independent and chemically different coordination complexes, mononuclear and binuclear in equal proportion. The structures of these complexes were investigated by single-crystal X-ray analysis, elemental analyses, NMR spectroscopy as well as electronic absorption and emission spectroscopy. The three complexes exhibit *in vitro* antitumor activity against human breast cancer cell line, MCF7.

Keywords: Triphenyltin chloride; Organodiimine ligand; Crystal structure; Antitumor

1. Introduction

Bio-organometallic chemistry has become a fruitful research field in the fight against cancer [1, 2]. Coordination and organometallic compounds are important antitumor agents. The initial evaluation of platinum-based anticancer drugs shifted to non-platinum metal-based agents because the clinical effectiveness of cisplatin is limited by significant side effects [3–11]. Many different metals, for example, Ti, Ga, Ge, Pd, Au, Co, Ru, and Sn, have minimized side effects associated with the use of platinum compounds as anticancer drugs [3–9]. Organotin(IV) complexes have shown interesting *in vivo* anticancer activity as new chemotherapy agents [12–15], binding to membrane proteins or glycoproteins, cellular proteins (e.g. to hexokinase, ATPase, acetylcholinesterase of human erythrocyte membrane or to skeletal muscle membranes) [16] or directly with DNA [17].

Organotin(IV) complexes containing aromatic nitrogen donors represent such complexes and several papers have dealt with their molecular structures [18–21]. Rigid rod-like organic ligands are usually employed to connect metal centers. In spite of the rich coordination chemistry exhibited by transition metals with these ligands [22, 23], relatively little is known about formal coordination of discrete organotin(IV)

*Corresponding author. Email: safaaetaiw@hotmail.com

ISSN 0095-8972 print/ISSN 1029-0389 online
http://dx.doi.org/10.1080/00958972.2012.725846

complexes with these ligands. Many organotin(IV) complexes of pyrazine have been characterized [24–28], however, few examples of 4,4′-bipyridine have been reported [29–31]. Here, we report the synthesis and characterization of three complexes of triphenyltin chloride with 4,4′-bipyridine, *trans*-1,2-bis(4-pyridyl)ethane and 1,2-bis(4-pyridyl)ethane.

2. Experimental

2.1. *Materials and characterization*

All reagents were commercially available and used as received. Microanalyses (C, H, and N) were carried out with a Perkin Elmer 2400 automatic elemental analyzer. IR spectra were recorded on a Bruker TENSOR 27 FT-IR spectrometer as KBr discs. Thermogravimetric analyses were carried out on a Shimadzu TGA-50H thermal analyzer (under N_2 atmosphere). Nuclear magnetic resonance spectra (^1H and ^{13}C) were recorded on a Bruker 600 MHz spectrometer at ambient temperature using DMSO-d_6.

2.2. *Syntheses*

Complexes **1**–**3** were prepared by the same procedure. Hot solution of 0.25 mmol L^{-1} of the bipodal ligand (78 mg bpy for **1**, 45.5 mg tbpe for **2** and 46 mg bpe for **3**) in 10 mL acetonitrile was added to hot solution of 96 mg (0.25 mmol L^{-1}) of Ph_3SnCl in 10 mL acetonitrile. Clear solution was obtained, from which colorless prismatic crystals of **1**–**3** started growing after one week. After filtration, the products were washed with small portions of cold water and MeCN and dried overnight. Anal. Calcd for **1** ($C_{51}H_{42}Cl_2N_3Sn_2$) (%): C, 60.93; H, 4.22; N, 4.18. Found (%): C, 60.99; H, 4.08; N, 4.11. IR spectrum (KBr disc, cm^{-1}): 3056 (m), 2945 (m), 1641 (s), 1602 (s), 1533 (w), 1475 (w), 1420 (m), 1069 (m), 1016 (s), 807 (m), 730 (s), 695 (s), 621 (m), 582 (w) and 454(s). Anal. Calcd for **2** ($C_{48}H_{40}Cl_2N_2Sn_2$) (%): C, 60.48; H, 4.23; N, 2.94. Found (%): C, 60.24; H, 4.12; N, 2.85. IR spectrum (KBr disc, cm^{-1}): 3056 (s), 3019 (sh), 2934 (m), 1645 (s), 1606 (m), 1560 (m), 1509 (m), 1476 (m), 1425 (s), 1212 (s), 1069 (s), 1001 (s), 839 (s), 730 (s), 696 (s), 552 (s) and 453 (s). Anal. Calcd for **3** ($C_{51}H_{42}Cl_2N_2Sn_2$) (%): C, 60.36; H, 4.43; N, 2.93. Found (%): C, 60.20; H, 4.36; N, 2.91. IR spectrum (KBr disc, cm^{-1}): 3055 (s), 2927 (w), 1644 (s), 1609 (m), 1567 (m), 1509 (m), 1473 (m), 1425 (s), 1301 (w), 1220 (s), 1069 (s), 1008 (s), 831 (s), 731 (s), 696 (s), 542 (s) and 452 (s).

2.3. *X-ray crystallography*

Single-crystal X-ray diffraction measurements were carried out on a Kappa CCD Enraf Nonius FR 90 four circle goniometer with graphite monochromated Mo-Kα radiation {[λMo-Kα] = 0.71073 Å} at 25 ± 2°C. The structures were solved using direct methods and all non-hydrogen atoms were located from the initial solution or from subsequent electron density difference maps during the initial stages of the refinement. After locating all of the non-hydrogen atoms in each structure the models were refined against F^2, first using isotropic and finally using anisotropic thermal displacement parameters.

Table 1. Crystal data and structure refinement parameters of **1–3**.

	1	**2**	**3**
Empirical formula	$C_{51}H_{42}Cl_2N_3Sn_2$	$C_{48}H_{40}Cl_2N_2Sn_2$	$C_{48}H_{42}Cl_2N_2Sn_2$
Formula weight	1005.22	953.148	955.164
Temperature (K)	298	298	298
Crystal system	Triclinic	Monoclinic	Monoclinic
Space group	$P\bar{1}$	$P2_1/c$	$P2_1/c$
Unit cell dimensions (Å, °)			
a	9.2216(6)	15.7703(3)	16.0210(4)
b	14.1125(12)	14.6467(3)	14.6182(3)
c	18.677(2)	19.1548(4)	19.1906(5)
α	82.857(4)	90.00	9.00
β	80.608(4)	102.3294(11)	103.5496(13)
γ	81.279(3)	90.00	90.00
Volume (Å^3), Z	2357.9(3), 2	4322.4(2), 4	4369.3(2), 4
Calculated density (Mg m^{-3})	1.396	1.465	1.452
Absorption coefficient (Mo-Kα) (mm^{-1})	1.21	1.31	1.30
R_{int}	0.073	0.063	0.029
Data/restraints/parameters	4581/0/523	3847/0/487	4885/0/505
Goodness of fit on F^2	3.052	1.565	1.852
R indices [$I > 3\sigma(I)$] R_1/wR_2	0.084/0.213	0.037/0.201	0.041/0.140
R indices (all data)	0.128/0.235	0.122/0.0208	0.118/0.170

The positions of the hydrogen atoms were then calculated and refined isotropically, and the final cycle of refinements was performed. Crystallographic data for **1–3** are summarized in table 1.

2.4. In vitro *antitumor activity*

In vitro cytotoxicity was tested using the method of Skehan *et al.* [32]. Complexes **1–3** dissolved in DMSO were subjected to cytotoxic evaluation against human breast adenocarcinoma cell line (MCF7). Cells were plated in a 96-multiwell plate (10^4 cells/well) for 24 h before treatment with the compound to allow attachment of cell to the wall of the plate. Different concentrations of the complex (0, 5, 12.5, 25, and 50 μg mL^{-1}) were added to the cell monolayer; triplicate wells were prepared for each individual dose. Monolayer cells were incubated with the compounds for 48 h at 37°C in 5% CO_2. After 48 h, cells were fixed, washed, and stained with Sulfo-Rhodamine-B stain. Excess stain was washed with acetic acid and attached stain was recovered with Tris EDTA buffer. The optical density of each well was measured by an ELISA reader at 564 nm. The absorbance data were converted to % cell viability. Wells containing untreated cells served as positive controls. The mean absorbance of the corresponding set of blanks was subtracted from the mean absorbance of wells incubated with each test agent. This value was then divided by the difference between the mean absorbance of the untreated cells and that of the blanks in order to calculate a percent inhibition for each concentration. The mean IC_{50} is the concentration of agent that reduces cell growth by 50% under the experimental conditions and is the average from at least three independent determinations. The relation between surviving fraction (% cell viability) and drug concentration is plotted to get the survival curve of the tumor cell line after

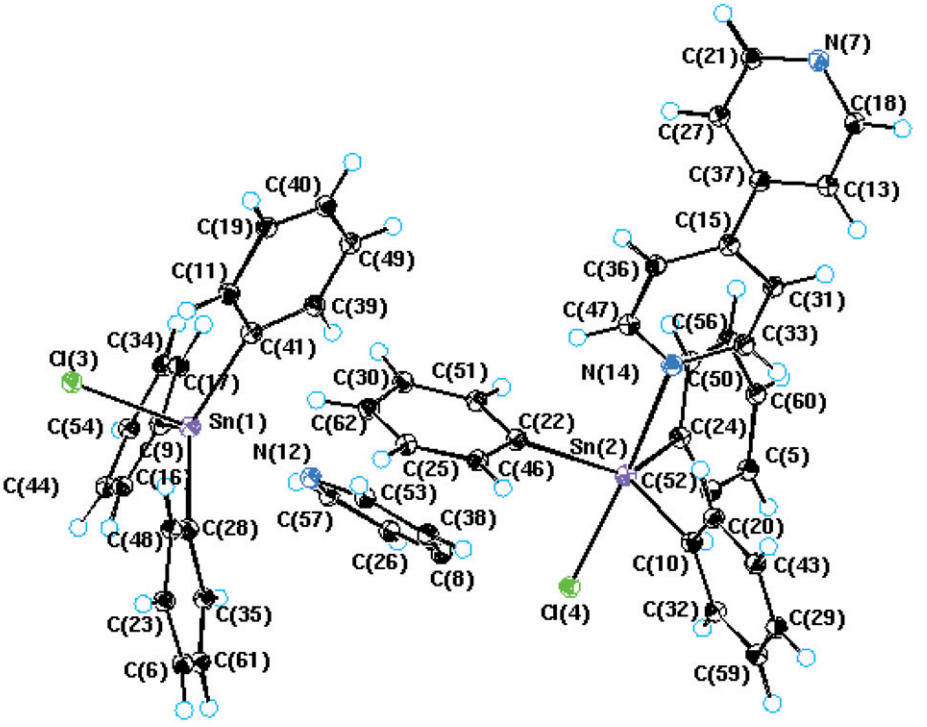

Figure 1. An ORTEP plot of the asymmetric unit of **1** showing the atom-numbering scheme.

application of the specified complex. The 50% inhibition concentration (IC_{50}) was determined by curve fitting.

3. Results and discussion

3.1. *Crystal structures of 1–3*

3.1.1. Crystal structure of 1. The asymmetric unit of **1** and atom-labeling scheme are shown in figure 1. The asymmetric unit cell of **1** consists of two crystallographically independent and chemically different coordination complexes A and B (figure 2). Thus, the structure of **1** contains two crystallographically distinct tins, Sn1 and Sn2. Sn2 of A is coordinated *via* three phenyl rings, one chloride, and one nitrogen atom, N14, from bipyridine forming a trigonal-bipyramidal configuration. The other nitrogen end, N7, of the bipyridine is free. The two pyridyl rings of 4,4′-bpy are not in the same plane, with a dihedral angle of 42.50°. The structure of B consists of centrosymmetric binuclear species with a bridging 4,4′-bpy. Sn1 is also trigonal bipyramidal with three phenyls forming the equatorial plane and one nitrogen of 4,4′-bpy and chloride occupying apical positions. Pyridyl rings are coplanar exhibiting 0° dihedral angle. In spite of the environments of Sn1 and Sn2 being essentially the same, the bond

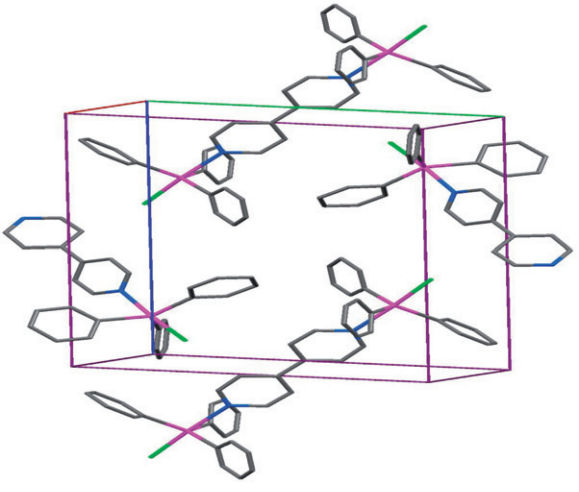

Figure 2. Content of the unit cell of **1**; hydrogen atoms are omitted for clarity.

Table 2. Selected bond lengths (Å) and angles (°) for **1**.

Sn1–Cl3	2.488(2)	N12–Sn1–C28	82.2(2)
Sn1–C9	2.122(5)	N12–Sn1–C41	86.8(2)
Sn1–N12	2.506(5)	C28–Sn1–C41	123.0(2)
Sn1–C28	2.131(6)	Cl4–Sn2–C10	93.3(2)
Sn1–C41	2.135(7)	Cl4–Sn2–N14	175.73(13)
Sn2–Cl4	2.514(2)	Cl4–Sn2–C22	88.2(2)
Sn2–C10	2.157(6)	Cl4–Sn2–C24	93.9(2)
Sn2–N14	2.461(5)	C10–Sn2–N14	88.3(2)
Sn2–C22	2.130(6)	C10–Sn2–C22	122.8(2)
Sn2–C24	2.142(6)	C10–Sn2–C24	117.0(2)
Cl3–Sn1–C9	100.3(2)	N14–Sn2–C22	87.6(2)
Cl3–Sn1–N12	174.97(12)	N14–Sn2–C24	88.8(2)
Cl3–Sn1–C28	93.6(2)	C22–Sn2–C24	120.0(2)
Cl3–Sn1–C41	93.1(2)	C9–Sn1–C28	120.1(2)
C9–Sn1–N12	84.3(2)	C9–Sn1–C41	114.0(2)

distances and angles are different (table 2). The bond lengths, Sn1–N12 = 2.506(5) Å, Sn2–N14 = 2.461(5) Å, Sn1–Cl3 = 2.488(2) Å, and Sn2–Cl4 = 2.514(2) Å are longer than those of prototype compounds [16, 20, 29, 30, 33], however, they are still shorter than the sum of the van der Waals radii of the two atoms, 3.72 Å [34]. The structure of B consists of discrete linear binuclear Cl–Sn–N–N–Sn–Cl with Cl–Sn–N angles deviating slightly from 180° (table 2). The extended structure of **1** consists of discrete units of A and B which run along the *a*-axis forming infinite parallel units with separation distance of 9.222 Å. These units are connected by extensive hydrogen bonds between the chloride and C–H (table 3; figures 3 and 4).

3.1.2. Crystal structure of 2. The empirical formula of **2** is $C_{48}H_{40}N_2Cl_2Sn_2$ and the chemical composition [$(Ph_3SnCl)_2$tbpe] was confirmed by single-crystal X-ray study.

Table 3. Hydrogen bonds (Å and °) for **1**.

D–H···A	D–H	H···A	D···A	∠D–H···A
C26^{i}–H26^{i}···Cl4	0.960	2.629(2)	3.567	165.81
C38–H38···Cl4	0.960	2.889(2)	3.848	177.69
C59^{i}–H59^{i}···Cl4	0.961	2.757(2)	3.675	160.21
C31^{ii}–H31^{ii}···N7	0.960	2.851(5)	3.642	140.31
C46^{iii}–H46^{iii}···N7	0.960	2.737(5)	3.406	127.29
C57–H57···C9	0.961	2.769(5)	3.291	114.89
C34–H34···C10	0.960	2.849(6)	3.677	145.06
C35–H35···N12	0.960	2.749(5)	3.159	106.50
C39–H39···N12	0.959	2.655(5)	3.215	117.71
C20–H20···N14	0.961	2.622(5)	3.211	119.96
C50–H50···N14	0.960	2.743(5)	3.262	114.57
C57–H57···C17	0.961	2.984(7)	3.653	127.88
C31–H31···C17	0.960	2.914(7)	3.585	127.83
C20–H20^{iii}···C21	0.961	2.940(7)	3.572	124.39
C47–H47···C22	0.960	2.706(6)	3.281	119.10
C16–H16···C29	0.959	2.863(7)	3.750	154.32
C56–H56···C34	0.960	2.936(7)	3.734	141.42
C16–H16···C43	0.959	2.908(7)	3.631	133.02
C56–H56···C44	0.960	2.907(7)	3.805	155.97
C47–H47···C46	0.960	2.908(7)	3.688	139.09
C50–H50···C56	0.960	2.907(7)	3.319	107.06
C49–H49···C48	0.9690	2.926(8)	3.805	152.70
C19^{iv}–H19^{iv}···C62	0.960	2.950(9)	3.881	163.50
C33–H33···C25	0.959	2.948(8)	3.703	136.45

Symmetry codes: $^{i}1-x,-y,-z$; $^{ii}-1-x,-y,1-z$; $^{iii}-x,-y,1-z$; $^{iv}1-x,-y,1-z$.

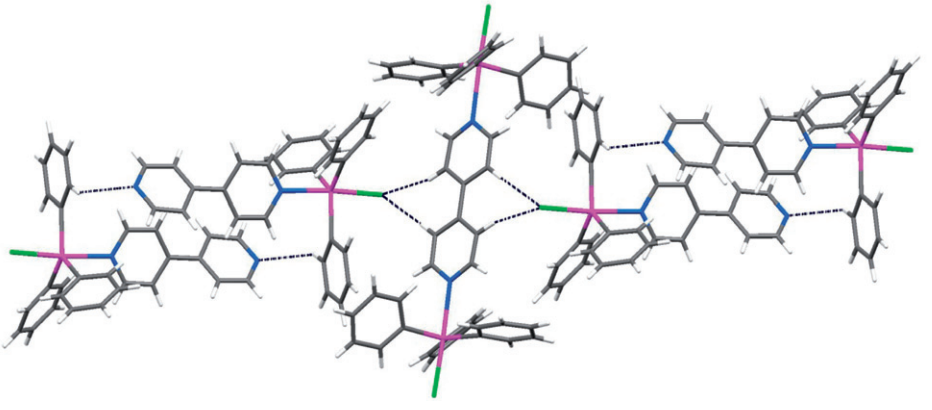

Figure 3. Association of the molecular units A and B of **1** by H-bonds.

The crystal data and structure refinement parameters of **2** are collected in table 1. The asymmetric unit of **2** contains one discrete molecule consisting of two crystallographically different Ph_3SnCl and one bridging tbpe (figure 5). The two pyridyl rings of tbpe are tilted by dihedral angle of 12.71°. The two Ph_3SnCl fragments are connected by tbpe forming a linear chain with the angles Cl3–Sn1–N5 = 178.04° and Cl3–Sn2–N13 = 176.27°. Sn–N bond distances, Sn1–N5 = 2.480 Å and Sn2–N13 = 2.482 Å, are longer than the reported values of similar compounds [16, 20, 33]. This elongation of Sn–N bond distances is due to the fact that the Sn atom is not

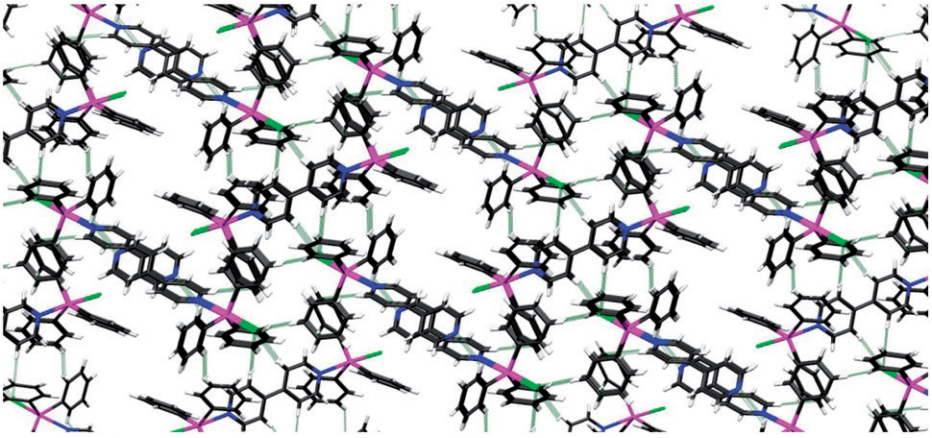

Figure 4. View of 3-D supramolecular structure of **1** along the *a*-axis; H-bonds are represented by dotted lines.

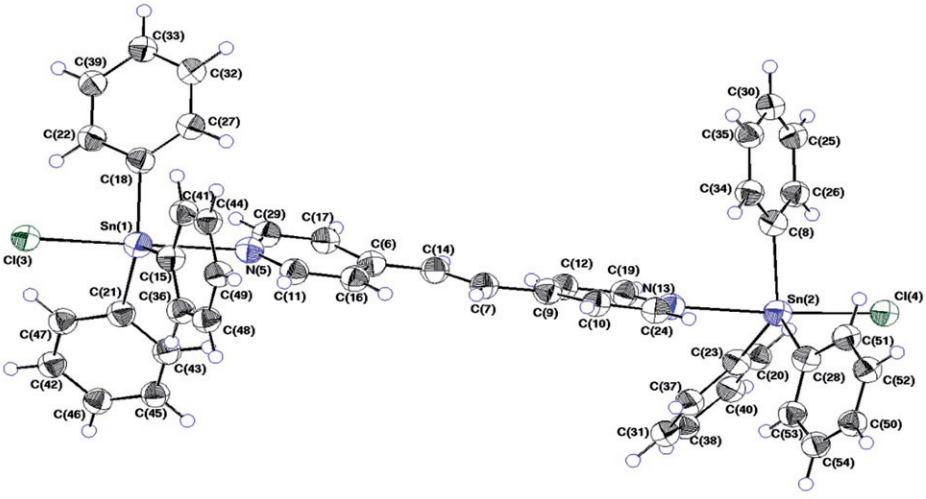

Figure 5. ORTEP plot of the asymmetric unit of **2** showing the atom-numbering scheme.

coordinated to two nitrogen atoms, but to one N and one Cl^-. However, the tin nitrogen bond lengths in **2** are equivalent. Each tin coordinates to equatorial phenyls and axial N and Cl^-. The phenyls are triangular with angles deviating slightly from 120° while axial N and Cl^- are at right angles to the Ph_3Sn plane (table 4). The ethylenic bond of tbpe exhibits the usual bond length of C7–C14 = 1.334 Å.

The extended structure of **2** consists of discontinuous 1-D chains, [Cl–Sn–N–N–Sn–Cl], which are arranged in a unique fashion creating a 2-D framework *via* conventional and non-conventional hydrogen bonds (table 5; figures 6 and 7). The hydrogen bonds represent the only supramolecular interaction in the structure of **2**.

Table 4. Selected bond lengths (Å) and angles (°) for **2**.

Sn1–Cl3	2.5190(9)	C15–Sn1–C21	121.01(13)
Sn1–N5	2.480(2)	C18–Sn1–C21	121.11(12)
Sn1–C15	2.129(3)	Cl4–Sn2–C8	92.22(9)
Sn1–C18	2.134(3)	Cl4–Sn2–N13	176.27(6)
Sn1–C21	2.151(3)	Cl4–Sn2–C23	95.52(9)
Sn2–Cl4	2.4787(8)	Cl4–Sn2–C28	92.69(9)
Sn2–C8	2.153(3)	C8–Sn2–N13	84.09(10)
Sn2–N13	2.482(2)	C8–Sn2–C23	121.40(12)
Sn2–C23	2.146(3)	C8–Sn2–C28	122.14(14)
Sn2–C28	2.143(3)	N13–Sn2–C23	86.01(10)
Cl3–Sn1–N5	178.04(7)	N13–Sn2–C28	89.70(11)
Cl3–Sn1–C15	93.28(8)	C23–Sn2–C28	115.39(14)
Cl3–Sn1–C18	93.59(8)	C15–Sn1–C18	116.71(13)
Cl3–Sn1–C21	93.88(9)	N5–Sn1–C18	86.39(10)
N5–Sn1–C15	84.98(10)	N5–Sn1–C21	87.80(11)

Table 5. Hydrogen bonds (Å and °) for **2**.

D–H···A	D–H	H···A	D···A	∠D–H···A
C7^{i}–H7^{i}···Cl3	0.960	2.8170(9)	3.765	169.56
C16^{i}–H16^{i}···Cl3	0.960	2.8214(9)	3.764	167.50
C14^{ii}–H14^{ii}···Cl4	0.959	2.8628(9)	3.771	158.28
C27–H27···N5	0.960	2.731(3)	3.222	112.44
C27–H27···C25	0.960	2.874(3)	3.730	149.03
C43–H43···N5	0.960	2.574(3)	3.173	120.59
C25^{iii}–H25^{iii}···C11	0.960	2.987(3)	3.786	141.39
C43–H43···C11	0.960	2.968(3)	3.794	144.89
C40^{iii}–H40^{iii}···C12	0.960	2.906(3)	3.742	146.26
C34–H34···N13	0.960	2.769(3)	3.199	108.06
C37–H37···N13	0.959	2.767(3)	3.235	110.84
C11–H11···C15	0.960	2.668(3)	3.238	118.50
C17^{ii}–H17^{ii}···C20	0.960	2.955(3)	3.682	133.48
C39^{iv}–H39^{iv}···C20	0.960	2.986(3)	3.711	133.35
C29^{ii}–H29^{ii}···C38	0.960	2.770(4)	3.676	157.76
C29^{ii}–H29^{ii}···C40	0.960	2.836(4)	3.684	117.41

Symmetry codes: $^{i}x,1/2-y,1/2+z$; $^{ii}x,1/2-y,z-1/2$; $^{iii}1-x,1/2+y,1/2-z$; $^{iv}1-x,-y,1-z$.

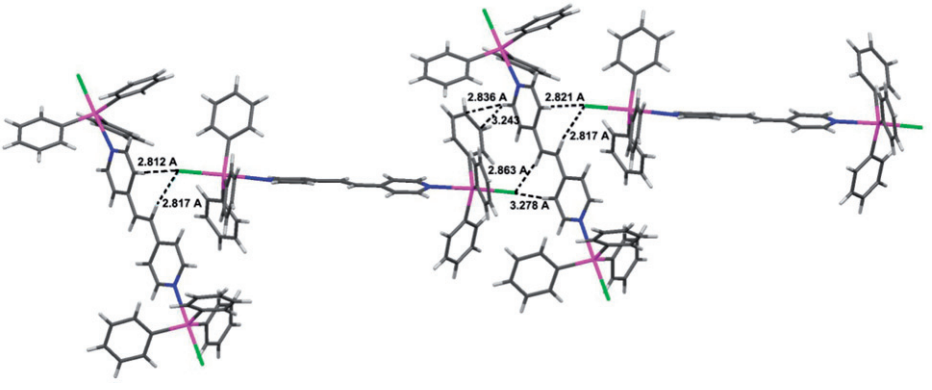

Figure 6. Association of the molecular units of **2** by H-bonds.

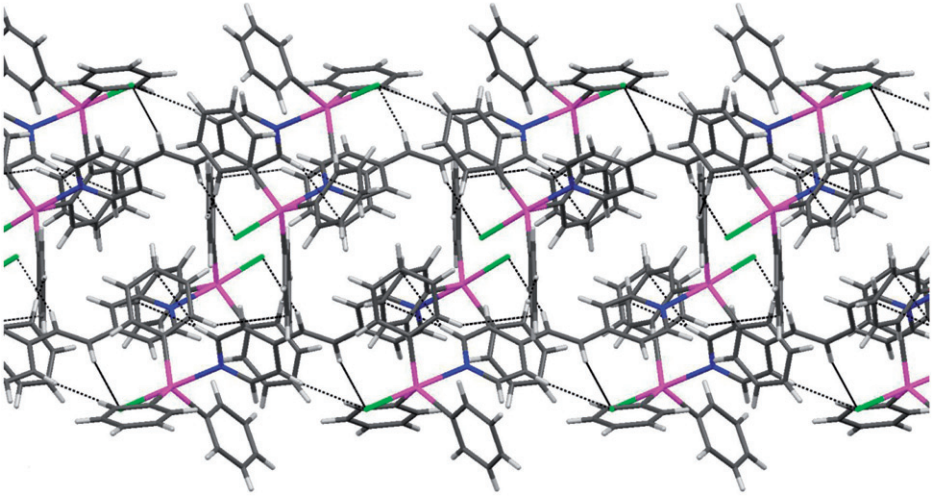

Figure 7. View of 2-D supramolecular structure of **2** along the *b*-axis; hydrogen bonds are represented by dotted lines.

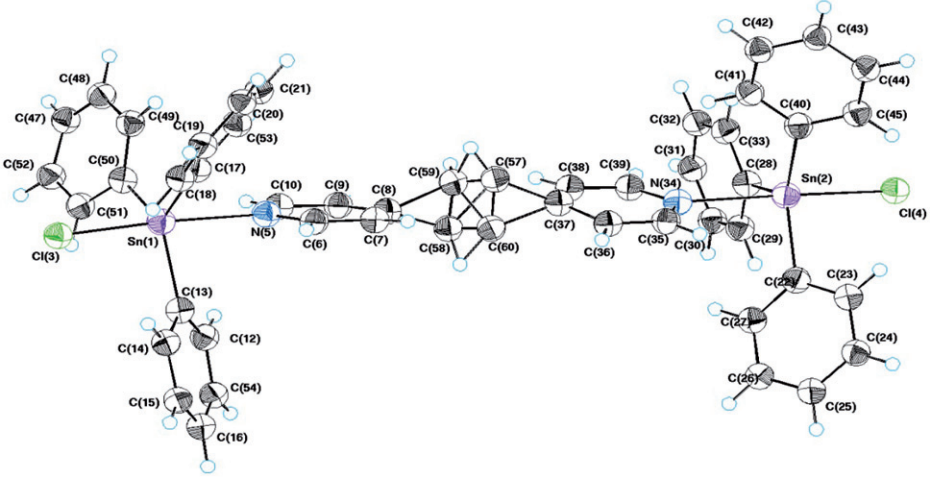

Figure 8. ORTEP plot of the asymmetric unit of **3** showing the atom-numbering scheme.

3.1.3. Crystal structure of 3. The ORTEP view of the unit cell of **3** with the atom-numbering scheme is shown in figure 8. The selected bond distances and angles of **3** are listed in table 6. The asymmetric unit of **3** comprises two Ph_3SnCl molecules interconnected by one bpe. Each tin is trigonal bipyramidal where three phenyls form the equatorial plane and one nitrogen atom of bpe and chloride occupy apical positions. The Cl–Sn distances are in the range of those observed in **1** and **2** while Sn–N distances are shorter (table 6). However, the Sn–N distances (2.470–2.496 Å) are still longer than the reported values (2.280–2.341 Å) [16, 20, 33]. The Cl–Sn–N angles are almost linear with a slightly bent structure, Cl3–Sn1–N5 = 176.37° and Cl4–Sn2–N34 = 177.47°.

Table 6. Selected bond lengths (Å) and angles (°) for **3**.

Sn1–Cl3	2.4791(6)	Cl3–Sn1–N5	176.37(6)
Sn1–N5	2.496(2)	Cl3–Sn1–C13	92.41(7)
Sn1–C13	2.143(3)	Cl3–Sn1–C17	95.38(7)
Sn1–C17	2.133(2)	Cl3–Sn1–C50	93.22(8)
Sn1–C50	2.140(3)	N5–Sn1–C13	84.03(8)
Sn2–Cl4	2.5151(7)	N5–Sn1–C17	85.86(8)
Sn2–N34	2.470(2)	N5–Sn1–C50	89.26(9)
Sn2–C22	2.133(3)	C13–Sn1–C17	120.47(10)
Sn2–C28	2.123(3)	C13–Sn1–C50	121.76(11)
Sn2–C40	2.146(3)	C17–Sn1–C50	116.56(12)
N34–Sn2–C28	85.37(8)	Cl4–Sn2–N34	177.47(5)
N34–Sn2–C40	88.38(9)	Cl4–Sn2–C22	93.14(7)
C22–Sn2–C28	116.56(12)	Cl4–Sn2–C28	92.61(7)
C22–Sn2–C40	121.23(10)	Cl4–Sn2–C40	93.97(8)
C28–Sn2–C40	121.26(12)	N34–Sn2–C22	86.42(8)

Table 7. Hydrogen bonds (Å and °) for **3**.

D–H···A	D–H	H···A	D···A	∠D–H···A
$C36^{i}$–$H36^{i}$···Cl3	0.960	2.9582(8)	3.845	154.21
$C38^{ii}$–$H38^{ii}$···Cl4	0.959	2.7269(7)	3.667	166.52
$C31^{iii}$–$H31^{iii}$···Cl4	0.960	2.9988(8)	3.804	142.27
C27–H27···N34	0.961	2.804(2)	3.260	109.97
C41–H41···N34	0.960	2.575(2)	3.189	121.93
C12–H12···N5	0.960	2.799(2)	3.214	107.03
C53–H53···N5	0.960	2.774(2)	3.224	109.44
C39–H39···C28	0.960	2.638(2)	3.213	118.89
C53–H53···C6	0.960	2.963(3)	3.228	97.26
$C35^{i}$–$H35^{i}$···C20	0.959	2.793(3)	3.709	159.79
C 19^{iv}–$H19^{iv}$···C7	0.960	2.901(4)	3.751	148.16
$C35^{i}$–$H35^{i}$···C19	0.959	2.821(4)	3.685	150.32
$C27^{iv}$–$H27^{iv}$···C15	0.961	2.871(3)	3.691	144.06
C10–H10···C50	0.960	2.982(3)	3.485	114.01
C6–H6···C53	0.961	2.991(3)	3.228	95.56

Symmetry codes: $^{i}x,1/2-y,z-1/2$; $^{ii}x,1/2-y,1/2+z$; $^{iii}1-x,-y,1-z$; $^{iv}1-x,1/2+y,1/2-z$.

Two pyridyl rings of bpe are nearly planar exhibiting dihedral angle of 12.28°. Dihedral angle of the two planes [Cl–Sn–pyridyl ring] is 11.98°. This forced coplanar structure of bpe causes unusual CH_2–CH_2 (ethane) linkage where the carbons occupy two crystallographically different positions with the occupancy of 0.5 (figure 8). The C59–C60 distance (1.363 Å) is shorter than the usual C–C bond distance while the C8(py)–C59 and C37(py)–C60 distances, 1.625 Å and 1.656 Å, respectively, are longer than the usual C–C bonds. The extended structure of **3** exhibits a 2-D framework *via* extensive hydrogen bonds (table 7; figure 9).

3.2. *NMR spectra of 1–3*

NMR spectra show the expected integration and peak multiplicities corresponding to the Ph_3Sn fragments and bidentate ligands. The spectra also showed only slight shifts of the peaks of the complexes compared to those of the free ligands (table 8). ^{1}H-NMR

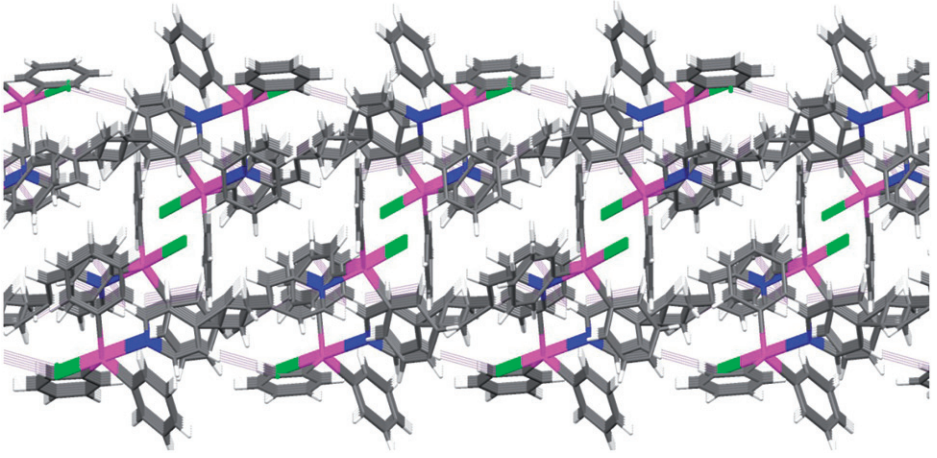

Figure 9. View of 2-D supramolecular structure of **3** along the *b*-axis; hydrogen bonds are represented by dotted lines.

Table 8. ^{13}C-NMR parameters of **1–3** and the free ligands.

Complex	δ (Ph–Sn)	$^{n}J(^{119/117}\text{Sn}-^{13}\text{C})$	δ (Ligand)	δ (Free ligand)
1	142.54 (C^{i})	780	120.12	121.24
	134.83 (C^{o})	45	143.36	144.08
	127.87 (C^{p})	Not observed	149.41	150.53
	127.24 (C^{m})	69		
2	143.65 (C^{i})	780	121.24	121.23
	135.95 (C^{o})	45	130. 55	130.54
	129.01 (C^{p})	Not observed	143.65	143.31
	128.38 (C^{m})	69	150.19	150.18
3	143.57 (C^{i})	780	34.48	34.48
	135.94 (C^{o})	45	123.92	123.92
	129.01 (C^{p})	Not observed	149.43	149.44
	128.38 (C^{m})	69	149.71	149.70

spectra of **1–3** display multiplets at $\delta = 7.39$–7.47 ppm corresponding to *meta*- and *para*-hydrogen atoms of Ph_3Sn, Supplementary figures S1–S3, whereas *ortho*-hydrogen atoms display a doublet at $\delta = 7.84$–7.87 ppm with its characteristic satellites due to spin coupling with ^{119}Sn and ^{117}Sn nuclei [$^{3}J(H^{m}–H^{o}) = 7.2$ Hz, $^{3}J(^{119/117}\text{Sn}–\text{H}^{o}) = 65$–$66$ Hz]. ^{1}H-NMR spectrum of **1** displays two distinct peaks for bpy (scheme 1). The doublet at 8.726–8.717 ppm, $^{3}J(H^{3}–H^{2}) = 4.8$ Hz, is assigned to $H_{2,6}$ and $H_{2',6'}$ while the doublet at 7.818–7.810 ppm is assigned to $H_{3,5}$ and $H_{3',5'}$. ^{1}H-NMR spectrum of **2** displays two doublets and one singlet for tbpe (scheme 1). The doublets at 8.620–8.618, $^{3}J(H^{3}–H^{2}) = 4.8$ Hz, and 7.625–7.617 ppm are assigned to $H_{2,6}$ and $H_{2',6'}$ and $H_{3,5}$ and $H_{3',5'}$, respectively. The singlet at 6.93 ppm is assigned to H_{7}, $H_{7'}$. ^{1}H-NMR spectrum of **3** displays a doublet at 8.455–8.447 ppm, $^{3}J(H^{3}–H^{2}) = 4.8$ Hz, due to $H_{2,6}$ and $H_{2',6'}$ while the doublet at 7.264–7.256 ppm is assigned to $H_{3,5}$ and $H_{3',5'}$ of bpe [35, 36]. The ethylenic group gives rise to one singlet band at 2.95 ppm. ^{13}C-spectra of **1–3** (table 8 and Supplementary figures S4–S6) display peaks due

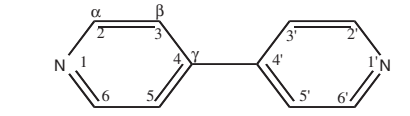

4,4'-Bipyridine

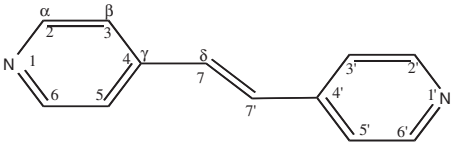

Trans-1,2-bis(4-pyridyl)ethylene

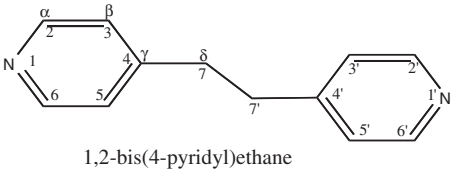

1,2-bis(4-pyridyl)ethane

Scheme 1. Structures and atom-numbering scheme of the bidentate aromatic ligands.

toPh_3Sn groups at $\delta = 127.24$–128.38, 127.87–129.01, 134.83–135.95, and 142.54–143.65 ppm due to *m*-C, *p*-C, *o*-C, and *i*-C atoms, respectively [37]. These peaks show considerable upfield shift of all carbon resonances compared with those of Ph_3SnCl. The bpy gives three singlets in the ^{13}C spectrum, at 120.12, 143.36, and 149.41 ppm, assigned to α, γ, and β carbon atoms, respectively. There are four peaks for tbpe in the ^{13}C-spectrum of **2**, at 121.24, 143.65, 150.19, and 130.55 ppm corresponding to β, γ, α, and the olefinic carbon nuclei, respectively [36, 38]. Also, there are four peaks for bpe at 123.92, 149.43, 149.71, and 34.48 ppm for β, γ, α, and the ethylenic carbon nuclei, respectively [36, 38]. The ^1H- and ^{13}C-NMR integration values were consistent with the formulation of the complexes. Thus, ^{13}C-NMR spectra of the ligands and Ph_3Sn display the expected carbon signals.

The use of NMR spectroscopy in study of structures of organotin compounds has increased [39, 40]. The coupling constants $^1J(^{119/117}Sn–^{13}C)$ depend markedly on the coordination number of tin and on the geometry of the coordination sphere. The coupling constants $^1J(^{119/117}Sn–^{13}C)$ for four-coordinate compounds are 550–660 Hz. The $^1J(^{119/117}Sn–^{13}C)$ values for the compounds with three phenyls in the equatorial plane and other ligands in axial positions are 750–850 Hz. Compounds with two phenyls in the equatorial plane and the third axial and the two donors of chelating ligand equatorial and axial have the coupling constants in the range of 600–660 Hz [39]. Chemical shifts and coupling constants $^1J(^{119/117}Sn–^{13}C)$ for **1**–**3** are shown in table 8. The values of $^1J(^{119/117}Sn–^{13}C)$ for the three complexes are 780 Hz, indicating that tin in the three complexes is five-coordinate in solution exhibiting trigonal-bipyramidal structure with three phenyls occupying equatorial positions.

^{119}Sn-NMR spectra were recorded and exhibit only one signal at -226.6 to -226.8 ppm (Supplementary figure S7), compatible with a five-coordinate geometry [41] in accordance with their structures in the solid state. These signals shift upfield with respect to that reported for Ph_3SnCl at -44.7 ppm [42].

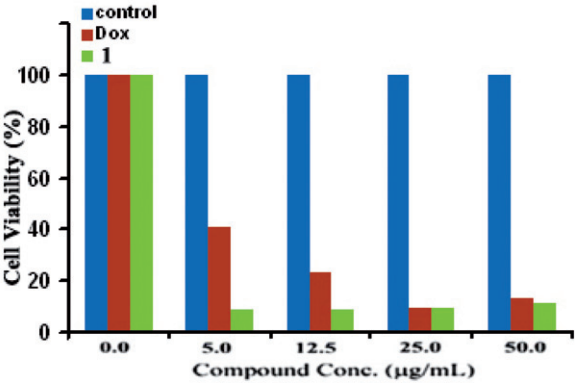

Figure 10. *In vitro* cytotoxicity of **1** and DOX against MCF7 human breast cancer cell line using different concentrations of **1** or DOX.
Untreated cells were used as mock. Each data point is an average of three independent experiments and expressed as $M \pm SD$.

3.3. *Thermal stability*

To evaluate the thermal stability of **1–3**, their thermogravimetric analyses were performed from 30°C to 800°C under N_2. The TGA curves of **1–3** show that the framework of these organotin complexes can be intact to 170–180°C. On further heating, **1–3** lose weight from 170°C to 290°C.

3.4. *In vitro effects of 1–3 on MCF7 human breast cancer cell line viability*

Breast cancer is the most common invasive malignancy and confounds treatment [43]. Novel treatments are urgently needed to improve the outcome for the large number of patients who relapse after receiving the currently available breast cancer therapies [44]. The triphenyltin chloride complexes were synthesized to examine the effects on proliferation of MCF7 human breast cancer cell line. Cell inhibition rates were determined by SRB assay. The results revealed that **1–3** inhibit the growth of MCF7 cells in a dose-dependent manner (figures 10–12). These complexes show inhibition of cell viability giving an IC_{50} value of $2.7\,\mu g\,mL^{-1}$, more inhibitory effects than Doxorubicin (DOX) ($IC_{50} = 4.35\,\mu g\,mL^{-1}$) and close to cisplatin ($IC_{50} = 1.4\,\mu g\,mL^{-1}$) [45] on MCF7 cell lines (figures 10–12). The tested compounds decreased cell viability of MCF7 cells compared to control group, but need more investigation *in vitro* and *in vivo*. Three primary factors are involved in structure–activity relationships for organotin(IV) complexes, $L_xR_nSnX_{4-n}$, the nature of the organic group {R}, of the halide or pseudohalide {X} and L. For active Sn complexes the average Sn–N bond lengths were > 239 pm, whereas inactive complexes had Sn–N bonds < 239 pm [46], implying that predissociation of the ligand may be important in the mode of action of these complexes, while coordinated ligand may favor transport of the active species to the site of action in the cells, where they are released by hydrolysis [46]. The IC_{50} value is the same for **1–3**, perhaps resulting from the fact that the Sn–N bond lengths are almost the same. The Sn–N bond lengths of these complexes are above 239 pm and they show higher cytotoxicity than the well-known drug, DOX.

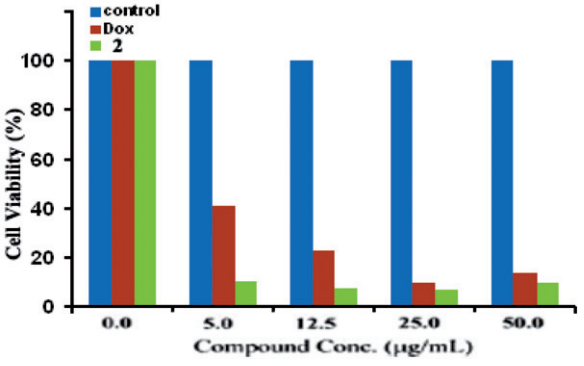

Figure 11. *In vitro* cytotoxicity of **2** and DOX against MCF7 human breast cancer cell line using different concentrations of **2** or DOX.
Untreated cells were used as mock. Each data point is an average of three independent experiments and expressed as $M \pm SD$.

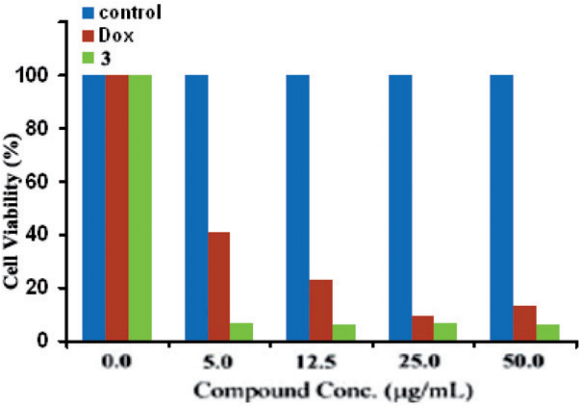

Figure 12. *In vitro* cytotoxicity of **3** and DOX against MCF7 human breast cancer cell line using different concentrations of **3** or DOX.
Untreated cells were used as mock. Each data point is an average of three independent experiments and expressed as $M \pm SD$.

4. Conclusion

Three complexes of triphenyltin chloride with bidentate N-donor aromatic ligands have been synthesized and structurally characterized. The length of the ligand plays an important role in assembly of these complexes; the product cannot be obtained with pyrazine. Complexes of tbpe and bpe are binuclear with ligands bridging two Ph_3SnCl molecules; bpy gave complicated structure consisting of two non-identical molecules; the first is mononuclear while the second is binuclear. The structure of **1** contains the same building blocks of $[(Ph_3SnCl)_2(4,4'\text{-bpy})_{1.5}(C_6H_6)_{0.5}]$ which contains benzene as a guest molecule [29]. Complexes **1**–**3** show high *in vitro* cytotoxicity against MCF7 cancer cell line and are promising candidates for further *in vivo* tests.

Supplementary material

Crystallographic data for the structural analyses have been deposited with the Cambridge Crystallographic Data Center, CCDC, Reference Nos CCDC 883 832–883834. These data can be obtained free of charge at www.ccdc.cam.ac.uk/conts/retrieving.html (or from the Cambridge Crystallographic Data Center, 12 Union Road, Cambridge CB21EZ, UK; Fax: +44 1223/336 033; E-mail: deposit@ccdc.cam.ac.uk).

References

[1] G.N. Kaluđerović, H. Kommera, E. Hey-Hawkins, R. Paschke, S. Gómez-Ruiz. *Metallomics*, **2**, 419 (2010).
[2] R.H. Fish, G. Jaouen. *Organometallics*, **22**, 2166 (2003).
[3] A. Alama, B. Tasso, F. Novelli, F. Sparatore. *Drug Discovery Today*, **14**, 500 (2009).
[4] M.A. Jakupec, M. Galanski, V.B. Arion, C.G. Hartinger, B.K. Keppler. *Dalton Trans.*, 183 (2008).
[5] S.K. Hadjikakou, N. Hadjiliadis. *Coord. Chem. Rev.*, **253**, 235 (2009).
[6] S.H. Etaiw, A.S. Sultan, A.S. Badr El-din. *Eur. J. Med. Chem.*, **46**, 5370 (2011).
[7] K. Strohfeldt, M. Tacke. *Chem. Soc. Rev.*, **37**, 1174 (2008).
[8] C.G. Hartinger, P.J. Dyson. *Chem. Soc. Rev.*, **38**, 391 (2009).
[9] P.C.A. Bruijnincx, P.J. Sadler. *Adv. Inorg. Chem.*, **61**, 1 (2009).
[10] P.C.A. Bruijnincx, P.J. Sadler. *Curr. Opin. Chem. Biol.*, **12**, 197 (2008).
[11] Y.K. Yan, M. Melchart, A. Habtemariam, P.J. Sadler. *Chem. Commun.*, 4764 (2005).
[12] I.I. Verginadis, S. Karkabounas, Y. Simos, E. Kontargiris, S.K. Hadjikakou, A. Batistatou, A. Evangelou, K. Charalabopoulos. *Eur. J. Pharm. Sci.*, **42**, 253 (2011).
[13] S.H. Etaiw, A.S. Sultan, M.M. El-bendary. *J. Organomet. Chem.*, **696**, 1668 (2011).
[14] M. Nath, S. Pokharia, R. Yadav. *Coord. Chem. Rev.*, **215**, 99 (2001).
[15] D. De Vos, R. Willem, M. Gielen, K.E. Van Wingerden, K. Nooter. *Met.-Based Drugs*, **5**, 179 (1998).
[16] L. Pellerito, L. Nagy. *Coord. Chem. Rev.*, **224**, 111 (2002).
[17] M.L. Falcioni, M. Pellei, R. Gabbianelli. *Mutat. Res. Genet. Toxicol. Environ. Mutagen.*, **653**, 57 (2008).
[18] T. Sedaghat, Z. Shokohi-pour. *J. Coord. Chem.*, **62**, 3837 (2009).
[19] M.A. Ali, A.H. Mirza, L.K. Wei, P.V. Bernhardt, O. Atchade, X. Song, G. Eng, L. May. *J. Coord. Chem.*, **63**, 1194 (2010).
[20] A. Azadmeher, M.M. Amini, N. Hadipour, H.R. Khavasi, H.-K. Fun, C.-J. Chen. *Appl. Organomet. Chem.*, **22**, 19 (2008).
[21] M.A. Salam, M.A. Affan, F.B. Ahmed, R.B. Hitam, Z. Gal. *J. Coord. Chem.*, **64**, 2409 (2011).
[22] Z. Fang, Q. Nie. *J. Coord. Chem.*, **64**, 2573 (2011).
[23] C.-S. Liu, E.C. Saňudo, M. Hu, Q. Zhang, L.-Q. Guo, S.-M. Fang. *J. Coord. Chem.*, **63**, 3393 (2010).
[24] E. Rivarola, M. Camalli, F. Caruso. *Inorg. Chim. Acta*, **126**, 1 (1987).
[25] D. Cunningham, P. McArdle, J. McManus, T. Higgins, K. Molloy. *J. Chem. Soc., Dalton Trans.*, 2621 (1988).
[26] J. McManus, D. Cunningham, M.J. Hynes. *J. Organomet. Chem.*, **468**, 87 (1994).
[27] D. Cunningham, J. McManus, M.J. Hynes. *J. Organomet. Chem.*, **393**, 69 (1990).
[28] E. Rivarola, A. Silvestri, R. Barbieri. *Inorg. Chim. Acta*, **28**, 223 (1978).
[29] C. Ma, J. Zhang, R. Zhang. *Heteroatom Chem.*, **15**, 338 (2004).
[30] S.W. Ng. *Acta Cryst.*, **C54**, 1393 (1998).
[31] S.A. Bajue, F.B. Bramwell, M. Charles, F. Cervantes-Lee, K. Pannell. *Inorg. Chim. Acta*, **197**, 83 (1992).
[32] P. Skehan, R. Storeng, D. Scudiero, A. Monks, J. McMahon, D. Vistica, J.T. Warren, H. Bokesch, S. Kenney, M.R. Boyd. *J. Natl. Cancer Inst.*, **82**, 1107 (1990).
[33] H.-D. Ying, C.-H. Wang, C.-L. Ma, Y. Wang. *Chin. J. Chem.*, **20**, 1129 (2002).
[34] A. Bondi. *J. Phys. Chem.*, **68**, 441 (1964).
[35] D.K. Lavellee, E.B. Fleischer. *J. Am. Chem. Soc.*, **94**, 2583 (1972).
[36] D.H. Willians, I. Fleming. *Spectroscopic Methods in Organic Chemistry*, 2nd Edn, McGraw-Hill, London (1973).
[37] F.P. Pruchnik, M. Banbula, Z. Ciunik, H. Chojnacki, M. Latocha, B. Skop, T. Wileczok, A. Opolski, J. Wietryk, A. Nasulewicz. *Eur. J. Inorg. Chem.*, 3214 (2002).
[38] J.M. Malin, C.F. Schmidt, H.E. Toma. *Inorg. Chem.*, **14**, 2924 (1975).
[39] J. Holeček, M. Nádvorník, K. Handlíř, A. Lyčka. *J. Organomet. Chem.*, **241**, 177 (1983).

[40] W. Rehman, A. Badshah, S. Khan, L.T.A. Tuyet. *Eur. J. Med. Chem.*, **44**, 3981 (2009).
[41] P. Chaudhary, M. Swami, D.K. Sharma, R.V. Singh. *Appl. Organomet. Chem.*, **23**, 140 (2009).
[42] J. Holecek, M. Nadvornik, K. Handlir, A. Lycka. *J. Organomet. Chem.*, **241**, 177 (1981).
[43] A.S. Sultan, J. Xie, M.J. LeBaron, L.E. Ealley, M.T. Nevalainen, H. Rui. *Oncogene*, **24**, 746 (2005).
[44] A.S. Sultan, H. Brim, Z.A. Sherif. *Cancer Sci.*, **99**, 272 (2008).
[45] R. Willem, A. Bouhdid, M. Biesemans, Jose C. Martins, D. de Vos, E.R.T. Tiekink, M. Gielen. *J. Organomet. Chem.*, **514**, 203 (1996).
[46] C. Pellerito, L. Nagy, L. Pellerito, A. Azorcsik. *J. Organomet. Chem.*, **691**, 1733 (2006).